






Cite this: *Phys. Chem. Chem. Phys.*,
2018, 20, 6187

Radiation-induced disorder in compressed lanthanide zirconates†

Sulgiye Park,  ^a Cameron L. Tracy, ^a Fuxiang Zhang, ^b Changyong Park,  ^c Christina Trautmann,  ^{de} Sergey N. Tkachev, ^f Maik Lang, ^g Wendy L. Mao ^{ah} and Rodney C. Ewing ^a

The effects of swift heavy ion irradiation-induced disordering on the behavior of lanthanide zirconate compounds ($\text{Ln}_2\text{Zr}_2\text{O}_7$ where $\text{Ln} = \text{Sm}, \text{Er}, \text{or Nd}$) at high pressures are investigated. After irradiation with 2.2 GeV ^{197}Au ions, the initial ordered pyrochlore structure ($Fd\bar{3}m$) transformed to a defect-fluorite structure ($Fm\bar{3}m$) in $\text{Sm}_2\text{Zr}_2\text{O}_7$ and $\text{Nd}_2\text{Zr}_2\text{O}_7$. For irradiated $\text{Er}_2\text{Zr}_2\text{O}_7$, which has a defect-fluorite structure, ion irradiation induces local disordering by introducing Frenkel defects despite retention of the initial structure. When subjected to high pressures (>29 GPa) in the absence of irradiation, all of these compounds transform to a cotunnite-like ($Pnma$) phase, followed by sluggish amorphization with further compression. However, if these compounds are irradiated prior to compression, the high pressure cotunnite-like phase is not formed. Rather, they transform directly from their post-irradiation defect-fluorite structure to an amorphous structure upon compression (>25 GPa). Defects and disordering induced by swift heavy ion irradiation alter the transformation pathways by raising the energetic barriers for the transformation to the high pressure cotunnite-like phase, rendering it inaccessible. As a result, the high pressure stability field of the amorphous phase is expanded to lower pressures when irradiation is coupled with compression. The responses of materials in the lanthanide zirconate system to irradiation and compression, both individually and in tandem, are strongly influenced by the specific lanthanide composition, which governs the defect energetics at extreme conditions.

Received 28th December 2017,
Accepted 6th February 2018

DOI: 10.1039/c7cp08664d

rsc.li/pccp

1. Introduction

Swift heavy ions (SHI) interact with matter primarily through the excitation of electrons. Having initial kinetic energies in the range of MeV–GeV, they deposit high electronic energy densities to a target material within less than a femtosecond, yielding far-from-equilibrium conditions.^{1–3} This electronic excitation and ionization (often expressed as an electronic energy loss per unit length, $(dE/dx)_e$), contrasts with the elastic nuclear collisions typical of lower ion energies.^{4–6} The modified interatomic forces accompanying this electronic excitation can render

accessible nonequilibrium phase transformation pathways within a nanometric region along the ion paths.⁷ When the structure or chemistry along the ion path are severely modified, a so-called ‘ion track’ is formed.^{5,8} The size and morphology of the nanoscale ion tracks depend on the properties of the material. Metals, semiconductors and insulators respond quite differently to high energy projectiles. Given that the irradiation conditions remain unchanged, ion tracks can be of fundamental interest for understanding basic material properties. The applications of swift heavy ion beams span a broad range, from electronic components for high-power electronics to semiconductor nanocomposites.^{9–11} Some specific examples of SHI irradiation-induced effects include dimensional changes in glassy metals,^{12,13} amorphization of crystalline materials,^{14,15} and shaping of nanoparticles through ion hammering.^{16–18} Thus, SHI irradiation is a promising technique that is applied to engineer, in a controlled manner, the atomic structure, and hence the physicochemical properties, of nanostructured materials. In addition to SHI irradiation, exposure of materials to high pressures can also modify the fundamental physical properties of materials such as their structures and bond-type. Compression effectively decreases the mean atomic volume and thus increases the electronic density, which, like SHI irradiation,

^a Department of Geological Sciences, Stanford University, Stanford, CA 94305, USA.
E-mail: sulgiye@stanford.edu

^b Materials Science and Technology Division, Oak Ridge National Laboratory, Oak Ridge, TN 37831, USA

^c HPCAT, Carnegie Institute of Washington, Argonne, IL 60439-4803, USA

^d GSI Helmholtzzentrum für Schwerionenforschung, 64291 Darmstadt, Germany

^e Technische Universität Darmstadt, 64287 Darmstadt, Germany

^f Center for Advanced Radiation Sources, University of Chicago, IL 60637, USA

^g Department of Nuclear Engineering, University of Tennessee, TN 37996, USA

^h Stanford Institute for Materials & Energy Sciences, SLAC National Accelerator Laboratory, Menlo Park, CA 94025, USA

† Electronic supplementary information (ESI) available. See DOI: 10.1039/c7cp08664d

modifies electronic structures and interatomic interactions, driving systems to far-from-equilibrium states and often yielding unique phases with unusual structures and chemistries.

Numerous SHI irradiation^{19–27} and high pressure^{28–35} studies have been performed on compounds in the complex oxide system $\text{Ln}_2\text{B}_2\text{O}_7$. These materials are particularly interesting as their structural modifications are highly dependent on the effects of composition on bonding, coordination, and the degrees of structural freedom.

At ambient conditions, $\text{Ln}_2\text{B}_2\text{O}_7$ compounds exhibit the pyrochlore structure ($Fd\bar{3}m$, $Z = 8$, unit cell parameter $a \approx 0.9\text{--}1.2\text{ nm}$) when the cation ionic radius ratio, r_A/r_B , is between ~ 1.46 and 1.78 .³⁶ The pyrochlore structure is closely related to the fluorite structure ($Fm\bar{3}m$), typical of AX_2 compounds, wherein each cation is in cubic 8-fold coordination. However, the pyrochlore structure is missing one-eighth of its anions, relative to the fluorite structure, and has two different, aliovalent cations ordered on the A- and B-sites.^{36,37} The pyrochlore A-site (16d) is typically occupied by large trivalent cations, such as lanthanides, actinides, or Y, in eight-fold coordination (coordinated with six 48f oxygen atoms and two 8b oxygen atoms). The B-site (16c) is occupied by smaller tetravalent transition metals, commonly Ti, Zr, or Hf, or group 14 element, such as Sn or Ge, in six-fold coordination (coordinated with six 48f oxygen atoms and two ordered 8a vacancies). There are two unique oxygen sites: the 48f oxygen is coordinated to two B^{4+} and two A^{3+} cations, and the 8b oxygen is coordinated with A^{3+} cations in a tetrahedral coordination.

The stability of this pyrochlore structure is often determined by the 48f oxygen positional parameter, x_{48f} , which is inversely proportional to r_A/r_B .³⁶ When r_A/r_B is below 1.46 (or x_{48f} is greater than 0.375), disordering into a defect-fluorite structure ($Fm\bar{3}m$) occurs.³⁶ This defect-fluorite structure exhibits a random distribution of the cations onto a face-centered cubic sublattice, and similar mixing of anions and vacancies over the tetrahedral interstices. Generally, the defect-fluorite structure can be considered a pyrochlore structure with high concentrations of cation antisite defects (mixing of the cations over the A- and B-sites) and anion Frenkel defects (mixing of anions and vacancies over the 48f, 8a, and 8b sites). However, recent investigations have shown that disordering is more complex than previously thought and the atomic configuration in a disordered pyrochlore is best modeled as a weberite-type structure rather than a defect-fluorite structure on a local scale.^{20,23,39} Overall, the compositional and structural flexibility of pyrochlore materials, as well as their unique, multiscale disordering mechanisms, lead to a broad range of applications in engineering and technology, including as matrices for immobilizing actinide elements from nuclear wastes;^{40–43} inert matrix nuclear fuels;⁴⁴ electrolytes in solid oxide fuel cells;⁴⁵ and thermal barrier coatings for gas turbine engines.⁴⁶

Previous investigations have shown that phase transformations in pyrochlore materials in response to irradiation are highly dependent on composition and the corresponding r_A/r_B value.^{21,22,41,47–50} The critical amorphization temperature (the temperature above which the thermal recrystallization rate is

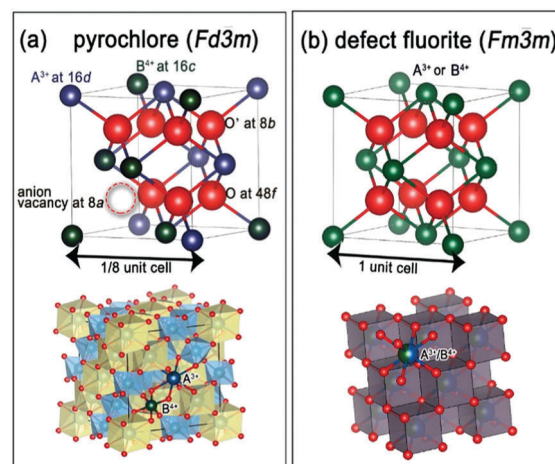


Fig. 1 Schematic diagrams of (a) the pyrochlore structure showing both 1/8 of a unit cell (top) and an entire unit cell (bottom) and (b) the defect-fluorite structure, which incorporates randomly-arranged anion vacancies (not shown). In the bottom illustrations, one polyhedron is omitted in each structure so as to illustrate the cation–anion bonding.

greater than the irradiation-induced amorphization rate) was found to increase with increasing r_A/r_B , which is attributed to the materials' inability to accommodate structural disorder due to an increased formation energy of antisite defects.^{20,23,26,51–53} In contrast, for compositions with low r_A/r_B , an order–disorder phase transformation to a defect-fluorite structure is typical under irradiation.^{20,25,54–57} This disordering in a pyrochlore series with low r_A/r_B is accompanied by a substantial change in the A-site environment.⁵⁸ A previous study using an extended X-ray absorption fine structure (EXAFS) spectroscopy has demonstrated that the most significant change upon ion irradiation is the decrease of interatomic distance in the nearest-neighbor oxygen atoms coordinating the A-site cation.⁵⁸ Additionally, this study showed that the next-nearest atoms coordinating both the A- and B-site cations are significantly disordered upon ion irradiation, which is likely a result from rotations about shared polyhedra edges and corners.⁵⁸ Fig. 1 shows the pyrochlore structure and its relation to this disordered, defect-fluorite structure.

Interestingly, similar compositional trends have been observed in the susceptibility of pyrochlore and defect-fluorite materials to phase transformations at high pressure. At ambient temperature, the high pressure behavior of many pyrochlore compounds involves a phase transformation to an orthorhombic cotunnite-like phase ($Pnma$).^{32–35,59,60} The critical pressure, P_{crit} (the pressure at which the phase transformation occurs), is lower for compounds with a defect-fluorite structure than it is for those with a pyrochlore structure due to the differing energetics of disordering.^{29,30,60} This differing high pressure response of the two structures to high pressure also extends to their behavior during decompression: compositions with lower r_A/r_B are commonly found to retain a defect-fluorite phase to ambient conditions, whereas those with higher r_A/r_B tend to amorphize upon pressure release.^{32–35,59,60} The contrasting stabilities of the high pressure phase in different pyrochlore compositions

with different initial structures have been attributed to the structural adjustments that accompany the different compositions.^{32–35,59,60} These structural adjustments are associated with substantial local strain. The local displacement of atoms from their ideal positions and/or rotations of polyhedra during disordering further displace adjacent atoms to create a larger displacement field, whose resulting average value affects the overall phase transitions.

Both pressure and irradiation-induced ionization offer a means for modifying the materials in this system by perturbing their electronic structures. These similarities have prompted some preliminary study on the combined effects of high pressure and ionization.^{61–63} Recently, Lang *et al.*¹ showed that the irradiation of a pyrochlore-structured material at >27 GPa yields the formation of a metastable phase with unique functional properties.¹ However, the high pressure behavior of materials in this system that have previously been modified by SHI irradiation has not been similarly studied. SHI irradiation-induced disordering alters the energy landscapes associated with the collective atomic motion necessary for high pressure phase transformations, which might dramatically alter the high pressure phase space, making this successive exposure to different extreme environments a potentially useful tool for synthesizing new phases. This study investigates the manner in which ion irradiation and subsequent exposure to high pressure affects the structural behavior of $\text{Ln}_2\text{Zr}_2\text{O}_7$ (where Ln = Nd, Sm, and Er) pyrochlore-type materials.

2. Experimental

Polycrystalline $\text{Ln}_2\text{Zr}_2\text{O}_7$ samples were synthesized from Ln_2O_3 and ZrO_2 powders by solid-state reaction at high temperature. The resulting powders were pressed into $\sim 2 \times 2$ mm-sized pellets with a hydraulic press at ~ 15 MPa and were fired at 1200 °C for 24 h. The pellets were then ground into fine powders (grain size ~ 1 μm) that were uniaxially pressed into low density compacts with a thickness of ~ 40 μm . The pressed powders were sintered at 800 °C for 24 h to remove any adsorbed water.

SHI irradiation was performed at beamline X0 of the UNILAC linear accelerator at the GSI Helmholtz Center for Heavy Ion Research in Darmstadt, Germany. All samples were simultaneously exposed, at room temperature and under vacuum, to a beam of ^{197}Au ions accelerated to 2.2 GeV. The projected range of the ion projectiles was calculated using the SRIM 2008 code,⁶⁴ the results of which are shown in Fig. 2. The average electronic energy loss $(dE/dx)_e$ scales with the density of a given material, and is thus higher for materials with smaller, heavier A-site cations ($\text{Nd}_2\text{Zr}_2\text{O}_7 \approx 37$ keV nm^{-1} ; $\text{Sm}_2\text{Zr}_2\text{O}_7 \approx 39$ keV nm^{-1} ; $\text{Er}_2\text{Zr}_2\text{O}_7 \approx 44$ keV nm^{-1}). The SRIM calculations indicate that all impinging ions passed through the samples (~ 40 μm thickness) with no implantation of Au. Within the samples, nuclear energy losses were several orders of magnitude lower than the electronic energy loss, and can be assumed to have negligible effect on the results of these experiments. The samples

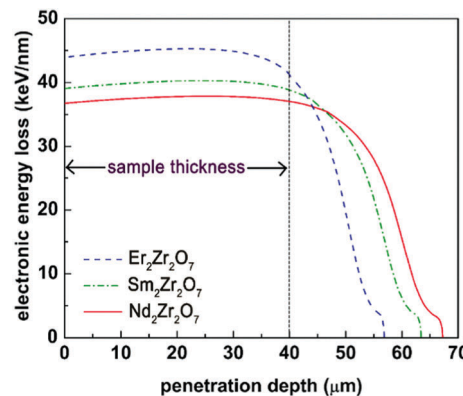


Fig. 2 Electronic energy loss of 2.2 GeV Au ions in $\text{Ln}_2\text{Zr}_2\text{O}_7$, where Ln = Er, Sm, and Nd, as a function of penetration depth calculated with the SRIM-2008 code.⁶⁴ All ions completely penetrate and exit the ~ 40 μm thick samples. The energy loss within the sample is nearly constant ($\pm \sim 1.8$ keV nm^{-1}).

were irradiated to fluences in the range 5×10^{10} – 3×10^{13} ions per cm^2 , with a typical fluence uncertainties of 10–15%. The ion flux was maintained below 2×10^9 ions per cm^2 per s to prevent bulk heating of the samples.

High pressure experiments were performed with symmetric diamond anvil cells (DACs). Rhenium gaskets were indented to a thickness of ~ 25 – 30 μm , and a hole with a diameter of 100–120 μm was drilled in the center to serve as a sample chamber. A small piece of the irradiated sample pellets and non-irradiated pristine pellets were loaded into the sample chambers. Neon gas was loaded into the sample chambers as a pressure-transmitting medium to promote hydrostaticity. Neon gas was chosen as it provides a much better hydrostatic environment and limited shear stresses even in solid phase compared with other common pressure media such as silicone oil or methanol–ethanol mixture.⁶⁵ Pressure in the DACs was determined using the standard ruby fluorescence method at room temperature.⁶⁶ Each high pressure experiment was duplicated at the synchrotron to obtain better statistics. All transformations were replicable using the same pressure medium.

Irradiation- and pressure-induced structural modifications were characterized using angle-dispersive synchrotron X-ray diffraction (XRD) at beamline 16-BM-D of the Advanced Photon Source (APS), Argonne National Laboratory (ANL). All samples were exposed to the ~ 25 μm diameter monochromatic X-ray beam in transmission geometry. Debye rings were recorded with a mar345 image plate detector. The detector images were integrated in the azimuthal direction using the software Dioplas.⁶⁷ Unit cell parameters were derived from Rietveld refinement of the observed XRD patterns using the Fullprof software.^{68,69} For all patterns, backgrounds were fit with a 6th-order polynomial and the diffraction peak profile was fit with pseudo-Voigt functions. Pressure–volume (P – V) curves were fit to a second-order Birch–Murnaghan equation of state (pressure-derivative of bulk modulus $B' = 4$) using EosFit7-GUI.^{70,71}

Irradiation-induced structural modifications were also investigated at ambient pressure using Raman spectroscopy,

which provides complementary information on changes to the short-range ordering and coordination. Spectra were collected using a Horiba Scientific LabRAM HR Evolution spectrometer at the NanoShared Facility at Stanford University. A $\lambda = 514.5$ nm HeNe laser source was used with a grating of 1800 l mm^{-1} to optimize the signal intensity. Each sample was exposed for 150 s and at least 4 scans were performed for each to ensure reasonable average spectra at each fluence.

3. Results and discussion

3.1 Swift heavy ion irradiation

A series of representative diffraction patterns of lanthanide zirconate compounds, irradiated to various ion fluences (increasing from bottom to top), are shown in Fig. 3. Patterns obtained from the unirradiated compounds exhibit well-crystallized pyrochlore phases for $\text{Nd}_2\text{Zr}_2\text{O}_7$ and $\text{Sm}_2\text{Zr}_2\text{O}_7$, and a defect-fluorite phase for $\text{Er}_2\text{Zr}_2\text{O}_7$, in line with their r_A/r_B ratios as described above. The differences in these two structures are evidenced by the presence or absence of the less-intense diffraction maxima corresponding to the ordering of the pyrochlore structure. These maxima include contributions from both the cation and anion ordering and appear at, for example, $2\theta \approx 4.8^\circ$, 12.1° , and 14.5° , which correspond to the planes (111), (133), and (155), respectively (Fig. 3). The intensity of these superstructure peaks decreases with increasing mass of the A-site cation, and decreasing r_A ($r_{\text{Nd}} > r_{\text{Sm}}$). The more-intense diffraction maxima, such as those at $2\theta = 9.7^\circ$ (222), 11.2° (004), 15.8° (044), and 18.6° (226) arise from fluorite substructure ordering, such that only these peaks appear for $\text{Er}_2\text{Zr}_2\text{O}_7$.

In all three compounds, the diffraction peak full width at half-maximum (FWHM) increases as a function of increasing fluence. William–Hall analysis⁷² indicates that the broadening of the diffraction maxima is caused by non-uniform strains (heterogeneous microstrain as opposed to the crystalline size decrease – see ESI,† Fig. S1), which can be attributed to structural deformation around defects and defect clusters created during ion energy deposition.^{19–26,51,73–77}

As a function of increasing ion fluence, $\text{Er}_2\text{Zr}_2\text{O}_7$ exhibits no substantial change in its long-range periodicity, and the

defect-fluorite structure is retained even at the highest fluence of 7×10^{13} ions per cm^2 . In contrast, $\text{Sm}_2\text{Zr}_2\text{O}_7$ and $\text{Nd}_2\text{Zr}_2\text{O}_7$, which initially exhibit the pyrochlore structure, disorder into defect-fluorite structures. This is evidenced by the disappearance of the less-intense maxima of the pyrochlore superstructure at a fluence 1×10^{12} ions per cm^2 . As the XRD intensities of the characteristic pyrochlore peaks diminish, the relative intensity of the (222) peak increases, and the remaining XRD peaks can be indexed as defect-fluorite structure. The loss of pyrochlore superstructure ordering is attributed to the mixing of A- and B-site cations onto a single sublattice, as well as the mixing of anion 8a vacancies on the other anion sublattice sites.²⁰ In $\text{Nd}_2\text{Zr}_2\text{O}_7$, diffraction peaks progressively decrease in intensity even after disordering into a defect-fluorite phase has finished. Concurrently, a weak diffuse scattering feature is observed between $2\theta \sim 9^\circ$ and 11° for fluences above 4×10^{12} ions per cm^2 . This diffuse scattering band indicates partial amorphization of $\text{Nd}_2\text{Zr}_2\text{O}_7$, consistent with the previous work of Sattonnay *et al.*, which demonstrated partial amorphization of $\text{Nd}_2\text{Zr}_2\text{O}_7$ irradiated with 120 MeV U ions.^{78,79} Since the current investigation was meant to elucidate the high-pressure behavior of the irradiation-induced defect-fluorite structure, fluences higher than 8×10^{12} ions per cm^2 , which would induce further amorphization, were avoided.

In addition to the XRD measurements, which provide information on the long-range periodicity of a material, Raman spectroscopy probes structures at the local scale, making it a useful, complementary tool to study changes to the coordination and defect characteristics of materials. A high degree of disorder in pyrochlore materials produced by SHI irradiation yields strong attenuation of signal from Raman-active vibrational modes. The Raman spectra of the three compounds as a function of increasing ion fluence are shown in Fig. 4. Factor group analysis of $\text{Ln}_2\text{B}_2\text{O}_7$ -type pyrochlores with the space group $Fd\bar{3}m$ predicts six Raman-active modes: $\Gamma = A_{1g} + E_g + 4F_{2g}$.^{58,80–82} The three most intense peaks are centered at Raman shifts of approximately 310 cm^{-1} , 390 cm^{-1} and 520 cm^{-1} , which are assigned to the O–A–O bending mode (E_{1g} and F_{2g}), B–O stretching mode with a mixture of A–O stretching and O–B–O bending vibrations (F_{2g}), and the A–O stretching mode (A_{1g}),

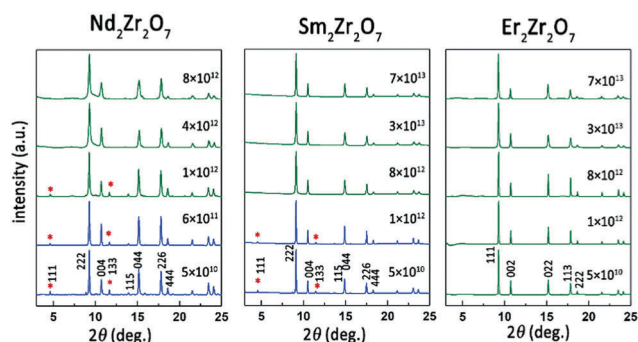


Fig. 3 Representative XRD patterns of $\text{Ln}_2\text{Zr}_2\text{O}_7$ compounds irradiated with 2.2 GeV Au ions at various fluences (X-ray wavelength $\lambda = 0.496 \text{ \AA}$). The unit for ion fluence is ions per cm^2 . Red asterisks indicate superstructure diffraction maxima typical of pyrochlore structure (blue indicates pyrochlore structure, green indicates defect-fluorite structure).

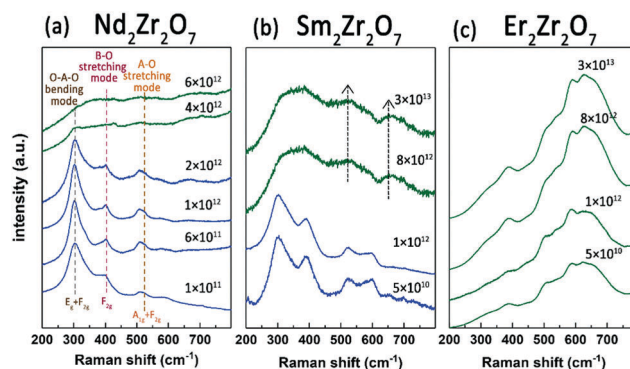


Fig. 4 Representative Raman spectra of lanthanide zirconate compounds for various 2.2 GeV Au ion fluences.

respectively (Fig. 4). The remaining pyrochlore Raman bands are relatively weak and only marginal signals belonging to the F_{2g} modes are found in the high wavenumber region.⁸³ Among the four F_{2g} modes, one of them arises from vibrations of the oxygen in the 8b site, while the others arise from 48f oxygen vibrations.⁸⁴

Upon irradiation, the intensity of the vibrational modes decreases for $\text{Nd}_2\text{Zr}_2\text{O}_7$ and $\text{Sm}_2\text{Zr}_2\text{O}_7$, which can be attributed to the strain-induced distortion of bonds concomitant with defect formation, in agreement with the XRD results.⁵² All prominent Raman bands of pyrochlore in $\text{Nd}_2\text{Zr}_2\text{O}_7$ and $\text{Sm}_2\text{Zr}_2\text{O}_7$ broaden substantially with increasing ion fluence. Concurrently, new broad bands centered at $\sim 500\text{ cm}^{-1}$ and $\sim 675\text{ cm}^{-1}$ appear and grow starting at fluences above 4×10^{12} ions per cm^2 . The attenuation of the pyrochlore modes in the Raman spectra confirms the loss of pyrochlore-type ordering as a result of dense electronic excitation. The growth of new bands is most likely an indication of the formation of the disordered defect-fluorite phase, as these bands resemble the vibration modes of defect-fluorite $\text{Er}_2\text{Zr}_2\text{O}_7$.

Materials with an ideal fluorite structure have comparatively simple vibrational spectra with one Raman-active phonon of F_{2g} symmetry.⁸³ The selection rules for Raman scattering are relaxed for the anion-deficient defect-fluorite structure, mainly due to the presence of vacancies on the oxygen sublattice and cation antisites.⁸³ For defect-fluorite materials, multiple broad Raman bands are typically observed. Hence, the Raman spectra obtained for $\text{Nd}_2\text{Zr}_2\text{O}_7$ and $\text{Sm}_2\text{Zr}_2\text{O}_7$ at high ion fluences are consistent with the XRD results, as the presence of several broad scattering features indicates a pyrochlore-to-defect-fluorite phase transformation. Comparison of the Raman spectra from all compounds at the highest ion fluences, when the irradiation-induced transformations are complete, shows that the spectra of $\text{Sm}_2\text{Zr}_2\text{O}_7$ and $\text{Nd}_2\text{Zr}_2\text{O}_7$ are qualitatively different from the spectrum of $\text{Er}_2\text{Zr}_2\text{O}_7$. The only common feature is the appearance of comparable bands centered at ~ 500 and 675 cm^{-1} . This indicates that the local structures of the irradiated pyrochlore and defect-fluorite compounds are distinct, despite having the same long-range structure. This is consistent with the observation by Shamblin *et al.* that the local structure of pyrochlores disordered by irradiation is indeed slightly different from that of the pyrochlore disordered by any other means.³⁹

The irradiation-induced order–disorder phase transition in zirconate pyrochlores is consistent with the results of previous studies.^{20,25,54–57} Earlier experiments and atomistic calculations validated that SHI bombardment produces point defects along the ion path, which causes an order–disorder transformation once a critical defect density is achieved.^{20,25,54–57} At this critical defect density, the oxygen in the 48f site shifts from its ideal tetrahedral position towards the equally-occupied A-site cations. This is favorable due to the vacancy in the 8a site of pyrochlores, which allows distortion of cation and anion polyhedra as cation interstitials relax onto the other cation site (cation antisite defect), and anion interstitials relax onto the vacant anion site, leaving another vacancy (anion Frenkel defect) (Fig. 5). The propensity of these materials to disorder depends

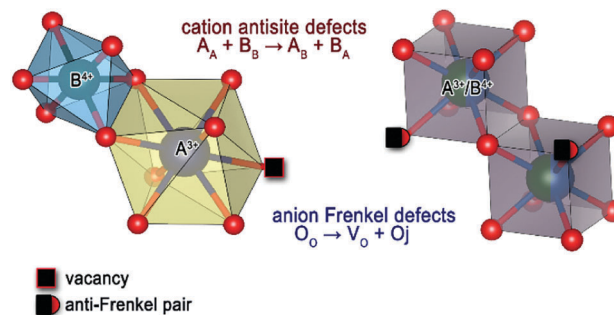


Fig. 5 Schematic illustration of the phase transformations from the pyrochlore structure ($Fd\bar{3}m$) to the defect-fluorite structure ($Fm\bar{3}m$) induced by cation antisite defect and anion Frenkel defect formation (adapted from ref. 85). The SHI irradiation-induced order–disorder phase transformation involves randomization of the anions in the 8a, 8b and 48f sites of the pyrochlore structure, as well as the cations in the 16c and 16d sites. This results in an average anion occupancy of 0.875 for each anion site.

on r_A/r_B , such that with a systematic decrease in the average A-to-B cation radius ratio, there is an increased tendency to disorder. Thus, materials in this system with smaller r_A/r_B tend to form a defect-fluorite structure, while those with larger r_A/r_B are more susceptible to ion beam-induced amorphization. This explains the slight amorphization observed in irradiated $\text{Nd}_2\text{Zr}_2\text{O}_7$, as opposed to $\text{Sm}_2\text{Zr}_2\text{O}_7$, which retained its crystallinity and merely disordered into a defect-fluorite structure.

3.2 High pressure behavior of unirradiated materials

Representative XRD patterns of unirradiated zirconate compounds at various pressures are shown in Fig. 6 (see ESI,† Fig. S2 for patterns with more pressure points). Regardless of the initial structure, all compositions exhibit the same general trends as a function of increasing pressure: (1) shifts of diffraction maxima to higher 2θ values; (2) broadening of the diffraction maxima; (3) the appearance of new diffraction maxima; and (4) the growth of broad, diffuse scattering bands. The shifts and gradual broadening

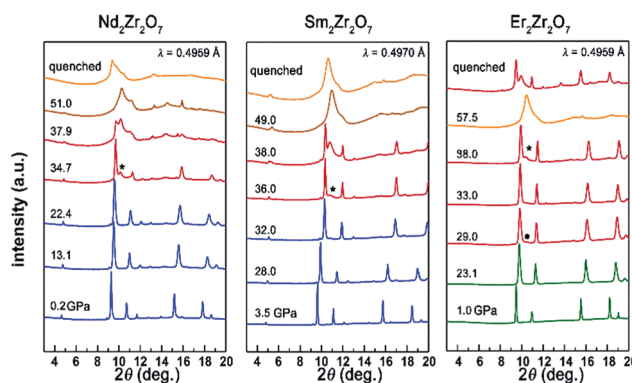


Fig. 6 Representative XRD patterns of unirradiated lanthanide zirconates as a function of pressure up to ~ 50 GPa. Numbers on the left are pressures in GPa. The critical pressure, P_{crit} , for the appearance of cotunnite-like phase in each compound is marked with asterisks. (For color codes: blue indicates pyrochlore structure, green indicates defect-fluorite structure, red indicates cotunnite-like phase, brown indicates a mixed amorphous and cotunnite-like phase, and orange indicates amorphous phase.)

of the diffraction maxima with increasing pressure indicate unit cell contraction and the accumulation of microstrain, both arising from compression of the powder crystallites. The growth of new diffraction maxima, concurrent with the disappearance of the initial peaks, indicates a pressure-induced phase transformation. In all compositions, this phase transformation is accompanied by partial amorphization, evidenced by the growth of diffuse scattering at higher pressures.

For all three compositions, XRD peaks corresponding to the initial cubic phases are fully retained up to ~ 30 GPa. For $\text{Nd}_2\text{Zr}_2\text{O}_7$ and $\text{Sm}_2\text{Zr}_2\text{O}_7$, for which the initial structure is pyrochlore, the high pressure phase transformations begin with the growth of a new peak between the (222) and (004) diffraction maxima at ~ 35 and ~ 36 GPa, respectively. The same phase transformation occurs for $\text{Er}_2\text{Zr}_2\text{O}_7$, where the growth of a new peak is now between (111) and (002), with an onset pressure of ~ 35 GPa. In addition to this phase transformation in $\text{Er}_2\text{Zr}_2\text{O}_7$, the (111) peak starts to become asymmetric at ~ 29 GPa, which may indicate a minor structural modification associated with the formation of the high pressure phase. The high pressure phase coexists with the initial cubic phases over a range of 10–15 GPa, indicating a kinetically-limited phase transformation. At pressures ≥ 50 GPa, the peaks corresponding to the high pressure phase become difficult to resolve, such that the patterns begin to resemble those of amorphous phases, which are dominated by diffuse scattering bands. Nevertheless, slight remnants of the crystalline peaks from the high pressure phase are observed, further reinforcing the sluggish kinetics of the transformation process. In the unirradiated samples, the overall structural responses of the three materials to compression are quite similar, except that the critical pressures for the transformations and response of the quenched phase are dependent on the initial structure.

The observed high pressure structural distortion is consistent with observations in the previous literature.^{29,32–35,59,85} The crystalline high pressure phase has been identified as a cotunnite-like orthorhombic phase (*Pnma*), isostructural with $\alpha\text{-PbCl}_2$, and has been reported as a high pressure polymorph in a wide range of $\text{Ln}_2\text{B}_2\text{O}_7$ compounds.^{29,32–35,59,85} In the cotunnite-like structure, the cations are 8- or 9-fold coordinated to oxygen, and are mixed on a single cation sublattice site, similar to the defect-fluorite structure. However, the presence of large strains, disorder, and random redistribution of cations and anions yield substantial broadening of the XRD peaks that, combined with the presence of an amorphous domain, make refinement of XRD patterns from this phase extremely challenging. First-principles calculations suggest that the formation of

the cotunnite-like phase is energetically-favored at high pressure as it has a lower formation enthalpy than the defect-fluorite or the compositionally-equivalent amorphous phase in a specific pressure range.^{35,86} Accompanying this structural transformation, the bonding in these materials changes at high pressure, in line with the increased ionicity of the cotunnite-like phase.³⁶

As with the irradiation-induced phase transition, the atomic-scale mechanism for this high pressure-induced modification is an order–disorder transition. Pressure causes defect accumulation, which in turn, induces a “swapping” of cations on the 16c and 16d sites, eventually yielding the solid solution cation sublattice required by the cotunnite-like phase.³⁰ Alongside antisite formation, the (111) cation planes buckle into adjacent anion planes, increasing their coordination and yielding an elastic anisotropy, which drives the system to form a non-cubic phase at high pressures.³⁶ For $\text{Ln}_2\text{B}_2\text{O}_7$ -type compounds, the defect accumulation depends on the antisite defect formation energy, which in turn, depends on r_A/r_B (*i.e.*, smaller mismatch of cation radii leads to a smaller energy for antisite formation), as well as the ionicity of B–O bonds. If the A-site cation strongly influenced this cubic-to-cotunnite phase transformation, the zirconate compounds with larger r_A could be expected to require higher pressures to transform to the high pressure phase (*i.e.*, $P_{\text{crit}}(\text{Nd}) > P_{\text{crit}}(\text{Sm})$). In this study, however, such a trend is not obvious for the two pyrochlore phases ($\text{Nd}_2\text{Zr}_2\text{O}_7$ and $\text{Sm}_2\text{Zr}_2\text{O}_7$), which have similar P_{crit} for formation of the cotunnite-like phase (Table 1). This suggests that, in the pyrochlore zirconate system, the A-site composition may play a limited role on the defect energetics. The difference of ~ 1 GPa in the P_{crit} for both compositions is within the error. The limited influence of the lanthanide elements in this transformation process is in agreement with previous literature³⁶ and is attributed to the comparable ionicity of the Zr–O bonds. Only when the A-site cation size is notably smaller and the Zr–O bond becomes much less ionic, then the P_{crit} is reduced, as is the case for $\text{Er}_2\text{Zr}_2\text{O}_7$, in agreement to its lower defect formation energy.

Upon pressure release, $\text{Nd}_2\text{Zr}_2\text{O}_7$ and $\text{Sm}_2\text{Zr}_2\text{O}_7$ retain their amorphous structures as evidenced by the absence of sharp Bragg peaks in patterns collected from the decompressed samples. In contrast, a crystalline structure is observed for $\text{Er}_2\text{Zr}_2\text{O}_7$ after pressure release; a mixture of the cotunnite-like high pressure phase and the initial defect-fluorite phase is recovered. Similar to the formation of the cotunnite-like phase, the recovery process of $\text{Er}_2\text{Zr}_2\text{O}_7$ is kinetically limited, and a small amount of the high pressure cotunnite-like phase is retained when quenched to ambient conditions. The different behavior of $\text{Er}_2\text{Zr}_2\text{O}_7$, compared with the other compounds, upon pressure

Table 1 Chemical composition, cation radius ratio (r_A/r_B), initial space group, 48f oxygen position parameter, x_{48f} , critical transition pressure (P_{crit}), high pressure phase, and bulk modulus (B_0), of pristine and SHI irradiated lanthanide zirconate compounds (when $B' = 4$). For B_0 , the number in brackets refers to the 1σ uncertainty in the last given digit

	r_A/r_B	Initial phase	x_{48f}	Pre-irradiation P_{crit} (GPa)	High pressure phase	B_0 (GPa)	Post-irradiation P_{crit} (GPa)	High pressure phase	B_0 (GPa)
$\text{Nd}_2\text{Zr}_2\text{O}_7$	1.56	<i>Fd3m</i>	0.332	34.7	<i>Pnma</i>	163.9 (5)	27.6	Amorphous	139.3 (4)
$\text{Sm}_2\text{Zr}_2\text{O}_7$	1.53	<i>Fd3m</i>	0.342	36.0	<i>Pnma</i>	168.8 (3)	31.0	Amorphous	153.7 (5)
$\text{Er}_2\text{Zr}_2\text{O}_7$	1.39	<i>Fm3m</i>	0.375	29.0	<i>Pnma</i>	193.8 (6)	25.4	Amorphous	174.7 (7)

release can also be understood in terms of their r_A/r_B . With larger A-site cation size mismatch, $\text{Nd}_2\text{Zr}_2\text{O}_7$ and $\text{Sm}_2\text{Zr}_2\text{O}_7$ have higher antisite formation energies, which contributes to an increased resistance to the formation of disordered phases (*i.e.* defect-fluorite or cotunnite-like structures). When cation antisite defects of the compressed sample exceed a critical value, the system cannot transform back to the ordered pyrochlore structure, resulting instead in an amorphous state upon structural relaxation.

3.3 High pressure behavior of irradiated materials

Representative high pressure XRD patterns of lanthanide zirconate compounds that have been subjected to SHI irradiation, such that those with the pyrochlore structure have been completely disordered into a defect-fluorite structure, are illustrated in Fig. 7 (see ESI,† Fig. S3 for patterns with more pressure points). A distinct difference is observed when compared to the unirradiated materials. The formation of the cotunnite-like phase at high pressure is inhibited for all compositions that have been irradiated with SHIs. Instead, the only phase transformation that occurs in the irradiated materials is evidenced by the appearance of significant asymmetry in the (111) diffraction maxima. This asymmetry grows into a diffuse scattering band, which is consistent with the presence of an amorphous phase. Since the more stable cotunnite-like phase is rendered inaccessible by irradiation-induced structural rearrangements, amorphization of all three compositions occurs gradually upon compression.

This inhibition of cotunnite-like (*Pnma*) phase formation in irradiated lanthanide zirconate compounds at high pressures is reported for the first time. The inaccessibility of the cotunnite-like phase suggests that SHI irradiation-induced electronic excitation yields structural modifications that alter the energy landscape at high pressure. While the cotunnite-like phase is energetically a more favorable phase than the non-irradiated cubic structures at these conditions, disordering and defect formation induced by ion irradiation increases the energetic barrier to its formation, rendering this high pressure phase

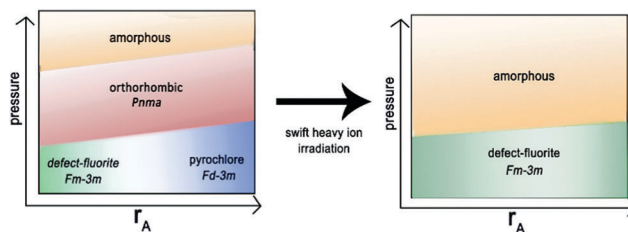


Fig. 8 Schematic representation of the stability field of lanthanide zirconates at high pressure. SHI irradiation extends the high pressure stability field of the amorphous phase to lower pressures, while also preventing the formation of the cotunnite-like phase.

kinetically inaccessible for the irradiated materials. This phenomenon can be understood as an extension of the high pressure metastability field of the amorphous phase to lower pressures after irradiation (Fig. 8). Upon the release of pressure, any compound with a defect-fluorite structure recovers this initial structure, regardless of the disordering or defects induced by SHI irradiation.

The change in the high pressure stability field of the irradiated materials is in agreement with previous findings.^{1,61,63} Lang *et al.*¹ and Schuster *et al.*⁶³ demonstrated a formation of a metastable phase¹ and an expansion of high-pressure stability range⁶³ by simultaneously irradiating the samples at high pressure. In another study, Lang *et al.*⁶¹ showed that only limited traces of the high pressure phase was found within a pressure range for which a non-irradiated samples was almost completely transformed.⁶¹ In agreement with these previous findings, the results reported in this study emphasize the radiation-induced microstructure changes that modify the critical pressure of phase transitions in materials. This is important as it highlights the different ways in which we can use the extreme parameters to manipulate and tune the properties of solids at the nanoscale.

Alongside its effects on phase formation, irradiation influences the compressibility of materials in this system (Fig. 9). The volume reduction in all three compounds as a function of pressure is comparable up to ~ 20 GPa, in the absence of irradiation. When irradiated prior to compression, all three materials become more

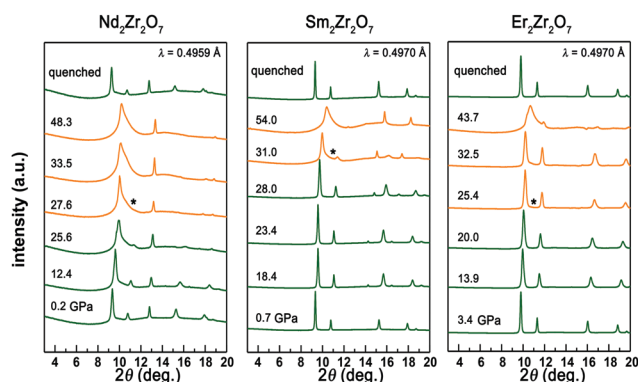


Fig. 7 Representative high pressure XRD patterns of zirconate compounds, after they had been completely disordered with SHI irradiation (at the highest applied fluence), up to pressures of ~ 50 GPa. Numbers on the left are pressures in GPa. The critical pressure, P_{crit} for the asymmetry in each compound is marked with asterisks.

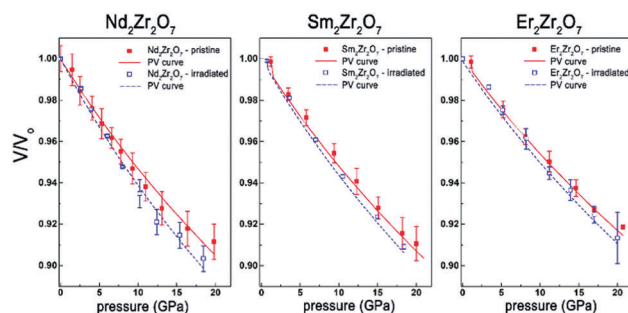


Fig. 9 Pressure–volume relationships for the three $\text{Ln}_2\text{Zr}_2\text{O}_7$ compounds studied. Volumes are derived from Rietveld refinement of high pressure XRD data. Error bars are obtained from the positional variation in the diffraction maxima. All data are fitted to the second-order Birch–Murnaghan equation of state. Solid red and dotted blue lines indicate PV curves of pristine and irradiated materials, respectively.

compressible. Fitting of the P - V data to a second-order Birch-Murnaghan equation of state^{87,88} shows that the bulk moduli of the irradiated compounds are lowered by ~ 10 – 15% (15–25 GPa) relative to those of the unirradiated compounds (Table 1). These lowered bulk moduli are consistent with the ~ 15 – 20% (5–7 GPa) decrease in the critical pressure for the onset of the transformation to a high pressure phase seen in the irradiated compositions, assuming that these transformations begin once a certain compression is achieved. These reductions in P_{crit} and bulk moduli indicates that SHI irradiation increases the energetic barrier for the formation of the high pressure cotunnite-like phase.

4. Conclusions

Upon irradiation with 2.2 GeV Au ions, $\text{Nd}_2\text{Zr}_2\text{O}_7$ and $\text{Sm}_2\text{Zr}_2\text{O}_7$ exhibited order-disorder phase transformations from the pyrochlore structure ($Fd\bar{3}m$) to the defect-fluorite structure ($Fm\bar{3}m$). This disordering is facilitated by their small $r_{\text{A}}/r_{\text{B}}$ which enhances the formation of both cation antisite defects and anion Frenkel defects. In $\text{Nd}_2\text{Zr}_2\text{O}_7$, wherein the $r_{\text{A}}/r_{\text{B}}$ is higher, minor amorphization was induced by ion irradiation. $\text{Er}_2\text{Zr}_2\text{O}_7$, for which the initial structure is already a defect-fluorite, exhibits no significant change in the long-range structure after irradiation.

Upon compression, all zirconate compositions transforms to a cotunnite-like high pressure phase ($Pnma$), followed by partial amorphization. However, when these materials are irradiated prior to exposure to high pressures, the formation of the cotunnite-like phase is inhibited. Irradiation-induced disordering and defect accumulation change the energy landscape associated with the high pressure transformations by increasing the activation energy required to form the cotunnite-like high pressure phase. As the materials cannot overcome the energy barrier to form a higher-density crystalline phase, they then lose their periodicity and become aperiodic. Additionally, the critical onset pressures for the loss of the initial low pressure phase and the bulk moduli decreased by ~ 15 – 20% and ~ 10 – 15% , respectively, in the irradiated materials, relative to the unirradiated materials.

The irradiation-induced modification of the phase stability fields of pyrochlore compounds at high pressures results from interplay between the introduction of nanoscale defects by dense electronic excitation, changes in bonding that accompany electron orbital overlap at high pressure, and the collective atomic motions associated with high pressure phase transformations. The study demonstrates that SHI irradiation makes accessible, at a given pressure, phases that cannot be achieved without the combination of these extreme environments.

Conflicts of interest

There are no conflicts of interest to declare.

Acknowledgements

S. G. Y. P. thanks S. Finkeldei for providing some of the pristine samples. This work was supported by the Energy Frontier

Research Center Materials Science of Actinides funded by the U.S. Department of Energy (DOE), Office of Science, Office of Basic Energy Sciences (Grant No. DE-SC0001089). Part of this work was performed at HPCAT (Sector 16), Advanced Photon Source (APS), Argonne National Laboratory. HPCAT operations are supported by DOE-NNSA under Award No. DE-NA0001974 and DOE-BES under Award No. DE-FG02-99ER45775, with partial instrumentation funding by NSF. The Advanced Photon Source is a U.S. Department of Energy (DOE) Office of Science User Facility operated for the DOE Office of Science by Argonne National Laboratory under Contract No. DE-AC02-06CH1135. Use of the Advanced Photon Source was supported by the Carnegie/Department of Energy Alliance Center (CDAC, DE-FC03-03NA00144).

References

- 1 M. Lang, F. Zhang, J. Zhang, J. Wang, B. Schuster, C. Trautmann, R. Neumann, U. Becker and R. C. Ewing, Nanoscale manipulation of the properties of solids at high pressure with relativistic heavy ions, *Nat. Mater.*, 2009, **8**, 793–797.
- 2 J. Wang, M. Lang, R. C. Ewing and U. Becker, Multi-scale simulation of structural heterogeneity of swift-heavy ion tracks in complex oxides, *J. Phys.: Condens. Matter*, 2013, **25**, 135001.
- 3 C. L. Tracy, M. Lang, J. Zhang, F. Zhang, Z. Wang and R. C. Ewing, Structural response of A_2TiO_5 ($\text{A} = \text{La}, \text{Nd}, \text{Sm}, \text{Gd}$) to swift heavy ion irradiation, *Acta Mater.*, 2012, **60**, 4477–4486.
- 4 F. F. Komarov, Defect and track formation in solids irradiated by superhigh-energy ions Defect and track formation in solids irradiated by superhigh-energy ions, *Phys.-Usp.*, 2003, **46**, 1253–1282.
- 5 N. Itoh, D. M. Duffy, S. Khakshouri and A. M. Stoneham, Making tracks: electronic excitation roles in forming swift heavy ion tracks, *J. Phys.: Condens. Matter*, 2009, **21**, 474205.
- 6 K. Schwartz, C. Trautmann and R. Neumann, Electronic excitations and heavy-ion-induced processes in ionic crystals, *Nucl. Instrum. Methods Phys. Res., Sect. B*, 2003, **209**, 73–84.
- 7 C. L. Tracy, M. Lang, F. Zhang, C. Trautmann and R. C. Ewing, Phase transformations in Ln_2O_3 materials irradiated with swift heavy ions, *Phys. Rev. B: Condens. Matter Mater. Phys.*, 2015, **92**, 174101.
- 8 D. M. Duffy, S. L. Daraszewicz and J. Mulroue, Modelling the effects of electronic excitations in ionic-covalent materials, *Nucl. Instrum. Methods Phys. Res., Sect. B*, 2012, **277**, 21–27.
- 9 S. Kuriakose, D. K. Avasthi and S. Mohapatra, Effects of swift heavy ion irradiation on structural, optical and photocatalytic properties of ZnO - CuO nanocomposites prepared by carbothermal evaporation method, *Beilstein J. Nanotechnol.*, 2015, **6**, 928–937.
- 10 M. Mishra, F. Meinerzhagen, M. Schleberger, D. Kanjilal and T. Mohanty, Swift Heavy Ion Induced Optical and Electronic Modifications of Graphene- TiO_2 Nanocomposites, *J. Phys. Chem. C*, 2015, **119**, 21270–21277.

- 11 C. Chen, L. Pang, Q. Lu, L. Wang, Y. Tan, Z. Wang and F. Chen, Refractive index engineering through swift heavy ion irradiation of LiNbO₃ crystal towards improved light guidance, *Sci. Rep.*, 2017, **7**, 10805.
- 12 M. Hou, S. Klaumünzer and G. Schumacher, Dimensional changes of metallic glasses during bombardment with fast heavy ions, *Phys. Rev. B: Condens. Matter Mater. Phys.*, 1990, **41**, 1144–1157.
- 13 W. Wesch, A. Kamarou and E. Wendler, Effect of high electronic energy deposition in semiconductors, *Nucl. Instrum. Methods Phys. Res., Sect. B*, 2004, **225**, 111–128.
- 14 A. Meftah, F. Brisard, J. M. Costantini, E. Dooryhee, M. Hage-Ali, M. Hervieu, J. P. Stoquert, F. Studer and M. Toulemonde, Track formation in SiO₂ quartz and the thermal-spike mechanism, *Phys. Rev. B: Condens. Matter Mater. Phys.*, 1994, **49**, 12457–12463.
- 15 B. Afra, M. Lang, M. D. Rodriguez, J. Zhang, R. Giulian, N. Kirby, R. C. Ewing, C. Trautmann, M. Toulemonde and P. Kluth, Annealing kinetics of latent particle tracks in Durango apatite, *Phys. Rev. B: Condens. Matter Mater. Phys.*, 2011, **83**, 064116.
- 16 C. D'Orléans, J. P. Stoquert, C. Estournès, C. Cerruti, J. J. Grob, J. L. Guille, F. Haas, D. Muller and M. Richard-Plouet, Anisotropy of Co nanoparticles induced by swift heavy ions, *Phys. Rev. B: Condens. Matter Mater. Phys.*, 2003, **67**, 220101.
- 17 R. Giulian, P. Kluth, L. L. Araujo, D. J. Sprouster, A. P. Byrne, D. J. Cookson and M. C. Ridgway, Shape transformation of Pt nanoparticles induced by swift heavy-ion irradiation, *Phys. Rev. B: Condens. Matter Mater. Phys.*, 2008, **78**, 125413.
- 18 P. Kluth, R. Giulian, D. J. Sprouster, C. S. Schnohr, A. P. Byrne, D. J. Cookson and M. C. Ridgway, Energy dependent saturation width of swift heavy ion shaped embedded Au nanoparticles, *Appl. Phys. Lett.*, 2009, **94**, 113107.
- 19 M. K. Patel, V. Vijayakumar, D. K. Avasthi, S. Kailas, J. C. Pivin, V. Grover, B. P. Mandal and A. K. Tyagi, Effect of swift heavy ion irradiation in pyrochlores, *Nucl. Instrum. Methods Phys. Res., Sect. B*, 2008, **266**, 2898–2901.
- 20 C. L. Tracy, J. Shamblin, S. Park, F. Zhang, C. Trautmann, M. Lang and R. C. Ewing, Role of composition, bond covalency, and short-range order in the disordering of stannate pyrochlores by swift heavy ion irradiation, *Phys. Rev. B*, 2016, **94**, 064102.
- 21 M. Lang, R. Devanathan, M. Toulemonde and C. Trautmann, Advances in understanding of swift heavy-ion tracks in complex ceramics, *Curr. Opin. Solid State Mater. Sci.*, 2015, **19**, 39–48.
- 22 G. Sattonnay, S. Moll, L. Thomé, C. Legros, A. Calvo, M. Herbst-Ghysel, C. Decorse and I. Monnet, Effect of composition on the behavior of pyrochlores irradiated with swift heavy ions, *Nucl. Instrum. Methods Phys. Res., Sect. B*, 2012, **272**, 261–265.
- 23 J. Shamblin, C. L. Tracy, R. C. Ewing, F. Zhang, W. Li, C. Trautmann and M. Lang, Structural response of titanate pyrochlores to swift heavy ion irradiation, *Acta Mater.*, 2016, **117**, 207–215.
- 24 G. Sattonnay, C. Grygiel, I. Monnet, C. Legros, M. Herbst-Ghysel and L. Thomé, Phenomenological model for the formation of heterogeneous tracks in pyrochlores irradiated with swift heavy ions, *Acta Mater.*, 2012, **60**, 22–34.
- 25 M. Lang, M. Toulemonde, J. Zhang, F. Zhang, C. L. Tracy, J. Lian, Z. Wang, W. J. Weber, D. Severin, M. Bender, C. Trautmann and R. C. Ewing, Swift heavy ion track formation in Gd₂Zr_{2–x}Ti_xO₇ pyrochlore: Effect of electronic energy loss, *Nucl. Instrum. Methods Phys. Res., Sect. B*, 2014, **336**, 102–115.
- 26 S. Park, M. Lang, C. L. Tracy, J. Zhang, F. Zhang, C. Trautmann, P. Kluth, M. D. Rodriguez and R. C. Ewing, Swift heavy ion irradiation-induced amorphization of La₂Ti₂O₇, *Nucl. Instrum. Methods Phys. Res., Sect. B*, 2014, **326**, 145–149.
- 27 S. Park, M. Lang, C. L. Tracy, J. Zhang, F. Zhang, C. Trautmann, M. D. Rodriguez, P. Kluth and R. C. Ewing, Response of Gd₂Ti₂O₇ and La₂Ti₂O₇ to swift-heavy ion irradiation and annealing, *Acta Mater.*, 2015, **93**, 1–11.
- 28 F. X. Zhang and S. K. Saxena, Structural changes and pressure-induced amorphization in rare earth titanates RE₂Ti₂O₇ (RE: Gd, Sm) with pyrochlore structure, *Chem. Phys. Lett.*, 2005, **413**, 248–251.
- 29 F. X. Zhang, M. Lang, U. Becker, R. C. Ewing and J. Lian, High pressure phase transitions and compressibilities of Er₂Zr₂O₇ and Ho₂Zr₂O₇, *Appl. Phys. Lett.*, 2008, **92**, 011909.
- 30 F. X. Zhang, J. W. Wang, J. Lian, M. K. Lang, U. Becker and R. C. Ewing, Phase stability and pressure dependence of defect formation in Gd₂Ti₂O₇ and Gd₂Zr₂O₇ pyrochlores, *Phys. Rev. Lett.*, 2008, **100**, 045503.
- 31 F. X. Zhang, B. Manoun and S. K. Saxena, Pressure-induced order–disorder transitions in pyrochlore RE₂Ti₂O₇ (RE = Y, Gd), *Mater. Lett.*, 2006, **60**, 2773–2776.
- 32 D. R. Rittman, K. M. Turner, S. Park, A. F. Fuentes, C. Park, R. C. Ewing and W. L. Mao, Strain engineered pyrochlore at high pressure, *Sci. Rep.*, 2017, **7**, 2236.
- 33 K. M. Turner, D. R. Rittman, R. A. Heymach and R. C. Ewing, Pressure-induced structural modifications of rare-earth hafnate pyrochlore, *J. Phys.: Condens. Matter*, 2017, **29**, 255401.
- 34 D. R. Rittman, K. M. Turner, S. Park, A. F. Fuentes, J. Yan, R. C. Ewing and W. L. Mao, High-pressure behavior of A₂B₂O₇ pyrochlore (A = Eu, Dy; B = Ti, Zr), *J. Appl. Phys.*, 2017, **121**, 045902.
- 35 H. Y. Xiao, F. X. Zhang, F. Gao, M. Lang, R. C. Ewing and W. J. Weber, Zirconate pyrochlores under high pressure, *Phys. Chem. Chem. Phys.*, 2010, **12**, 12472–12477.
- 36 M. A. Subramanian, G. Aravamudan and G. V. Subba Rao, Oxide pyrochlores—A review, *Prog. Solid State Chem.*, 1983, **15**, 55–143.
- 37 B. C. Chakoumakos, Systematics of the pyrochlore structure type, ideal A₂B₂X₆Y, *J. Solid State Chem.*, 1984, **53**, 120–129.
- 38 D. M. Strachan, R. D. Scheele, E. C. Buck, J. P. Icenhower, A. E. Kozelisky, R. L. Sell, R. J. Elovich and W. C. Buchmiller, Radiation damage effects in candidate titanates for Pu disposition: Pyrochlore, *J. Nucl. Mater.*, 2005, **345**, 109–135.

- 39 J. Shamblin, M. Feygenson, J. Neuefeind, C. L. Tracy, F. Zhang, S. Finkeldei, D. Bosbach, H. Zhou, R. C. Ewing and M. Lang, Probing disorder in isometric pyrochlore and related complex oxides, *Nat. Mater.*, 2016, **15**, 507–512.
- 40 S. Wang, L. Wang, R. C. Ewing, G. Was and G. Lumpkin, Ion irradiation-induced phase transformation of pyrochlore and zirconolite, *Nucl. Instrum. Methods Phys. Res., Sect. B*, 1999, **148**, 704–709.
- 41 K. E. Sickafus, L. Minervini, R. W. Grimes, J. a. Valdez, M. Ishimaru, F. Li, K. J. McClellan and T. Hartmann, Radiation Tolerance of Complex Oxides, *Science*, 2000, **289**, 748–751.
- 42 W. J. Weber, R. C. Ewing, C. R. A. Catlow, T. D. de la Rubia, L. W. Hobbs, C. Kinoshita, H. Matzke, A. T. Motta, M. Nastasi, E. K. H. Salje, E. R. Vance and S. J. Zinkle, Radiation effects in crystalline ceramics for the immobilization of high-level nuclear waste and plutonium, *J. Mater. Res.*, 1998, **13**, 1434–1484.
- 43 R. C. Ewing, W. J. Weber and J. Lian, Nuclear waste disposal-pyrochlore ($A_2B_2O_7$): Nuclear waste form for the immobilization of plutonium and ‘minor’ actinides, *J. Appl. Phys.*, 2004, **95**, 5949–5971.
- 44 S. Lutique, D. Staicu, R. J. M. Konings, V. V. Rondinella, J. Somers and T. Wiss, Zirconate pyrochlore as a transmutation target: thermal behaviour and radiation resistance against fission fragment impact, *J. Nucl. Mater.*, 2003, **319**, 59–64.
- 45 E. R. Andrievskaya, Phase equilibria in the refractory oxide systems of zirconia, hafnia and yttria with rare-earth oxides, *J. Eur. Ceram. Soc.*, 2008, **28**, 2363–2388.
- 46 J. Wu, X. Wei, N. P. Padture, P. G. Klemens, M. Gell, E. Garcíá, P. Miranzo and M. I. Osendi, Low-thermal-conductivity rare-earth zirconates for potential thermal-barrier coating applications, *J. Am. Ceram. Soc.*, 2002, **85**, 3031–3035.
- 47 J. Zhang, M. Lang, R. C. Ewing, R. Devanathan, W. J. Weber and M. Toulemonde, Nanoscale phase transitions under extreme conditions within an ion track, *J. Mater. Res.*, 2010, **25**, 1344–1351.
- 48 C. L. Tracy, M. Lang, J. M. Pray, F. Zhang, D. Popov, C. Park, C. Trautmann, M. Bender, D. Severin, V. A. Skuratov and R. C. Ewing, Redox response of actinide materials to highly ionizing radiation, *Nat. Commun.*, 2015, **6**, 6133.
- 49 G. Sattonnay, S. Moll, L. Thomé, C. Decorse, C. Legros, P. Simon, J. Jagielski, I. Jozwik and I. Monnet, Phase transformations induced by high electronic excitation in ion-irradiated $Gd_2Zr_xTi_{1-x}O_7$ pyrochlores, *J. Appl. Phys.*, 2010, **108**, 103512.
- 50 G. Sattonnay, M. Lahrichi, F. Garrido, L. Thomé, G. Sattonnay and M. Lahrichi, Stress field induced by swift heavy ion irradiation in cubic yttria stabilized zirconia, *J. Appl. Phys.*, 2007, **101**, 1–7.
- 51 S. Park, M. Lang, C. L. Tracy, J. Zhang, F. Zhang, C. Trautmann, M. D. Rodriguez, P. Kluth and R. C. Ewing, Response of $Gd_2Ti_2O_7$ and $La_2Ti_2O_7$ to swift-heavy ion irradiation and annealing, *Acta Mater.*, 2015, **93**, 1–11.
- 52 W. J. Weber and N. J. Hess, Ion beam modification of $Gd_2Ti_2O_7$, *Nucl. Instrum. Methods Phys. Res., Sect. B*, 1993, **80–81**, 1245–1248.
- 53 J. Lian, J. Chen, L. Wang, R. Ewing, J. Farmer, L. Boatner and K. Helean, Radiation-induced amorphization of rare-earth titanate pyrochlores, *Phys. Rev. B: Condens. Matter Mater. Phys.*, 2003, **68**, 134107.
- 54 S. X. Wang, B. D. Begg, L. M. Wang, R. C. Ewing, W. J. Weber and K. V. G. Kutty, Radiation stability of gadolinium zirconate: A waste form for plutonium disposition, *J. Mater. Res.*, 1999, **14**, 4470–4473.
- 55 Q. Xu, W. Pan, J. Wang, C. Wan, L. Qi, H. Miao, K. Mori and T. Torigoe, Rare-earth zirconate ceramics with fluorite structure for thermal barrier coatings, *J. Am. Ceram. Soc.*, 2006, **89**, 340–342.
- 56 J. Lian, K. B. Helean, B. J. Kennedy, L. M. Wang, A. Navrotsky and R. C. Ewing, Effect of structure and thermodynamic stability on the response of lanthanide stannate-pyrochlores to ion beam irradiation, *J. Phys. Chem. B*, 2006, **110**, 2343–2350.
- 57 R. Devanathan, W. J. Weber and J. D. Gale, Radiation tolerance of ceramics—insights from atomistic simulation of damage accumulation in pyrochlores, *Energy Environ. Sci.*, 2010, **3**, 1551.
- 58 N. J. Hess, B. D. Begg, S. D. Conradson, D. E. McCreedy, P. L. Gassman and W. J. Weber, Spectroscopic Investigations of the Structural Phase Transition in $Gd_2(Ti_{1-y}Zr_y)_2O_7$ Pyrochlores, *J. Phys. Chem. B*, 2002, **106**, 4663–4677.
- 59 K. M. Turner, C. L. Tracy, W. L. Mao and R. C. Ewing, Lanthanide stannate pyrochlores ($Ln_2Sn_2O_7$; $Ln = Nd, Gd, Er$) at high pressure, *J. Phys.: Condens. Matter*, 2017, **29**, 504005.
- 60 F. X. Zhang, J. Lian, U. Becker, L. M. Wang, J. Hu, S. Saxena and R. C. Ewing, Structural distortions and phase transformations in $Sm_2Zr_2O_7$ pyrochlore at high pressures, *Chem. Phys. Lett.*, 2007, **441**, 216–220.
- 61 M. Lang, F. Zhang, J. Lian and C. Trautmann, Combined high pressure and heavy-ion irradiation: a novel approach, *Synchrotron Radiat.*, 2009, **16**, 773–777.
- 62 U. A. Glasmacher, M. Lang, H. Keppler, F. Langenhorst, R. Neumann and D. Schardt, Phase Transitions in Solids Stimulated by Simultaneous Exposure to High Pressure and Relativistic Heavy Ions, *Phys. Rev. Lett.*, 2006, **96**, 195701.
- 63 B. Schuster, M. Lang, R. Klein, C. Trautmann, R. Neumann, A. Benyagoub, F. Fujara, B. Schuster, M. Lang, R. Klein, C. Trautmann and R. Neumann, Structural phase transition in ZrO_2 induced by swift heavy ion irradiation at high pressure, *Nucl. Instrum. Methods Phys. Res., Sect. B*, 2009, **267**, 964.
- 64 J. F. Ziegler, M. D. Ziegler and J. P. Biersack, SRIM – The stopping and range of ions in matter, *Nucl. Instrum. Methods Phys. Res., Sect. B*, 2010, **268**, 1818–1823.
- 65 S. Klotz, J.-C. Chervin, P. Munsch and G. Le Marchand, Hydrostatic limits of 11 pressure transmitting media, *J. Phys. D: Appl. Phys.*, 2009, **42**, 075413.
- 66 H. K. Mao, J. Xu and P. M. Bell, Calibration of the ruby pressure gauge to 800 kbar under quasi-hydrostatic conditions, *J. Geophys. Res.*, 1986, **91**, 4673.

- 67 C. Prescher and V. B. Prakapenka, DIOPTAS: a program for reduction of two-dimensional X-ray diffraction data and data exploration, *High Press. Res.*, 2015, **7959**, 1–8.
- 68 J. Rodriguez-Carvajal, Recent developments of the program FULLPROF, *Comm. Powder Diffraction (IUCr) Newslett.*, 2001, **26**, 12–19.
- 69 T. Roisnel and J. Rodriguez-Carvajal, WinPLOTR: A Windows Tool for Powder Diffraction Pattern Analysis, *Mater. Sci. Forum*, 2001, **378–381**, 118–123.
- 70 R. J. Angel, J. Gonzales-Platas and M. Alvaro, *EosFit7c and a Fortran module (library) for equation of state calculations*, De Gruyter, 2014, vol. 229, pp. 405–419.
- 71 J. Gonzales-Platas, M. Alvaro, F. Nestola and R. J. Angel, EosFit7-GUI: a new graphical user interface for equation of state calculations, analyses and teaching computer programs EosFit7-GUI: a new graphical user interface for equation of state calculations, analyses and, *J. Appl. Crystallogr.*, 2016, **49**, 1377–1382.
- 72 G. K. Williamson and W. H. Hall, X-ray line broadening from fcc aluminium and wolfram, *Acta Metall.*, 1953, **1**, 22–31.
- 73 P. Kluth, C. S. Schnorr, O. H. Pakarinen, F. Djurabekova, D. J. Sprouster, R. Giulian, M. C. Ridgway, A. P. Byrne, C. Trautmann, D. J. Cookson, K. Nordlund and M. Toulemonde, Fine Structure in Swift Heavy Ion Tracks in Amorphous SiO₂, *Phys. Rev. Lett.*, 2008, **101**, 175503.
- 74 A. Benyagoub, Phase transformations in oxides induced by swift heavy ions, *Nucl. Instrum. Methods Phys. Res., Sect. B*, 2006, **245**, 225–230.
- 75 M. Tang, P. Kluth, J. Zhang, M. K. Patel, B. P. Uberuaga, C. J. O. Reichhardt and K. E. Sickafus, Swift heavy ion irradiation-induced microstructure modification of two delta-phase oxides: Sc₄Zr₃O₁₂ and Lu₄Zr₃O₁₂, *Nucl. Instrum. Methods Phys. Res., Sect. B*, 2010, **268**, 3243–3247.
- 76 M. K. Patel, V. Vijayakumar, S. Kailas, D. K. Avasthi, J. C. Pivin and A. K. Tyagi, Structural modifications in pyrochlores caused by ions in the electronic stopping regime, *J. Nucl. Mater.*, 2008, **380**, 93–98.
- 77 M. Lang, F. Zhang, J. Zhang, J. Wang, J. Lian, W. J. Weber, B. Schuster, C. Trautmann, R. Neumann and R. C. Ewing, Review of A₂B₂O₇ pyrochlore response to irradiation and pressure, *Nucl. Instrum. Methods Phys. Res., Sect. B*, 2010, **268**, 2951–2959.
- 78 G. Sattonnay, L. Thomé, I. Monnet, C. Grygiel and C. Legros, Effects of electronic energy loss on the behavior of Nd₂Zr₂O₇ pyrochlore irradiated with swift heavy ions, *Nucl. Instrum. Methods Phys. Res., Sect. B*, 2012, **286**, 254–257.
- 79 G. Sattonnay, N. Sellami, L. Thome, C. Legros, C. Grygiel, I. Monnet, J. Jagielski, I. Jozwik-Biala and P. Simon, Structural stability of Nd₂Zr₂O₇ pyrochlore ion-irradiated in a broad energy range, *Acta Mater.*, 2013, **61**, 6492–6505.
- 80 M. T. Vandenborre, U. P. M. Curie, P. Jussieu, P. Cedex, E. Husson, J. P. Chatry, C. De Recherche, E. Centrale and D. Michel, Rare-earth Titanates and Stannates of Pyrochlore Structure; Vibrational Spectra and Force Fields, *J. Raman Spectrosc.*, 1983, **14**, 63–71.
- 81 H. C. Gupta, S. Brown, N. Rani and V. B. Gohef, A lattice dynamical investigation of the Raman and the infrared frequencies of the cubic A₂Hf₂O₇ pyrochlores, *J. Phys. Chem. Solids*, 2002, **63**, 535–538.
- 82 D. Michel and R. Collongues, Study by Raman spectroscopy of order-disorder phenomena occurring in some binary oxides with fluorite-related structures, *J. Raman Spectrosc.*, 1976, **5**, 163–180.
- 83 M. Glerup, O. Faurkov Nielsen and F. Willy Poulsen, The Structural Transformation from the Pyrochlore Structure, A₂B₂O₇, to the Fluorite Structure, AO₂, Studied by Raman Spectroscopy and Defect Chemistry Modeling, *J. Solid State Chem.*, 2001, **160**, 25–32.
- 84 T. T. A. Lummen, I. P. Handayani, M. C. Donker, D. Fausti, G. Dhalenne, P. Berthet, A. Revcolevschi and P. H. M. Van Loosdrecht, Phonon and crystal field excitations in geometrically frustrated rare earth titanates, *Phys. Rev. B: Condens. Matter Mater. Phys.*, 2008, **21**, 214310.
- 85 F. X. Zhang, M. Lang and R. C. Ewing, Atomic disorder in Gd₂Zr₂O₇ pyrochlore, *Appl. Phys. Lett.*, 2015, **106**, 191902.
- 86 H. Y. Xiao, F. Gao and W. J. Weber, *Ab initio* investigation of phase stability of Y₂O₇ and Y₂Zr₂O₇ under high pressure, *Phys. Rev. B: Condens. Matter Mater. Phys.*, 2009, **80**, 212102.
- 87 F. Birch, Finite Elastic Strain of Cubic Crystals, *Phys. Rev.*, 1947, **71**, 809–824.
- 88 F. Birch, Equation of State and Thermodynamic Parameters of NaCl to 300 kbar in the High-Temperature Domain, *J. Geophys. Res.*, 1986, **91**, 4949–4954.